JTTEE5 20:1217–1230
DOI: 10.1007/s11666-011-9669-2
1059-9630/$19.00 © ASM International

Wear Behavior of Plasma-Sprayed Carbon Nanotube-Reinforced Aluminum Oxide Coating in Marine and High-Temperature Environments

Anup Kumar Keshri and Arvind Agarwal

(Submitted February 12, 2011; in revised form June 11, 2011)

Wear behavior of plasma-sprayed carbon nanotube (CNT)-reinforced aluminum oxide (Al_2O_3) composite coatings are investigated at room temperature (298 K), elevated temperature (873 K), and in sea water. Lowest wear volume loss was observed in the sea water as compared to dry sliding at 298 and 873 K. Relative improvement in the wear resistance of Al_2O_3-8 wt.% CNT coating compared to Al_2O_3 was 72% at 298 K, 76% at 873 K, and 66% in sea water. The improvement in the wear resistance of Al_2O_3-CNT coatings is attributed to (i) larger area coverage by protective film on the wear surface at room temperature and in sea water, (ii) higher fracture toughness of Al_2O_3-CNT coatings due to CNT bridging between splats, and (iii) anti-friction effect of sea water. The average coefficient of friction (COF) was the lowest (0.55) in sea water and the highest (0.83) at 873 K for Al_2O_3-8 wt.% CNT coating.

Keywords carbon nanotube, friction and wear, nanocrystalline composites, nanopowders, nanostructured coatings, plasma spraying, wear mechanisms

1. Introduction

Plasma-sprayed aluminum oxide (Al_2O_3) coatings offer excellent wear resistance, corrosion resistance, heat, and thermal shock resistance, and have been widely used by the US Navy and other industries (Ref 1-6). These coatings have to operate under severe conditions, such as high load, high speed, elevated temperature, and aggressive corrosive and marine environments (Ref 5, 7-10). Therefore, it is of primary importance to study the tribological behavior of coatings at extreme conditions.

Tribological behavior of carbon nanotube (CNT)-reinforced Al_2O_3 composites has been explored earlier (Ref 8, 11-15). Ahmad et al. investigated the tribological behavior of hot-pressed Al_2O_3-CNT composites against silicon nitride (Si_3N_4) ball for varying CNT contents up to 10 wt.% (Ref 11). Addition of 10 wt.% of CNT in monolithic Al_2O_3 showed an improvement of 63% in sliding wear resistance under normal load of 14 N (Ref 11). This improvement was attributed to the dispersion of CNTs in Al_2O_3 matrix, CNT bridging within the Al_2O_3 grains, and strengthening of the grain boundaries by CNTs (Ref 11). An et al. also studied the tribological performance of hot-pressed Al_2O_3-CNT against Si_3N_4 ball and found that wear resistance improved for 4 wt.% CNT but showed deterioration at higher CNT content (10 wt.%) because of inhomogeneous dispersion and poor cohesion of CNT (Ref 12). Lim et al. showed that wear resistance continuously improved with an increase in CNT content up to 12 wt.% in Al_2O_3-CNT composite (Ref 15). This was attributed to the enhanced dispersion of CNTs in Al_2O_3 which was achieved by tape casting followed by lamination and hot pressing (Ref 15).

In our group's earlier study, Balani et al. reported the room temperature tribological behavior of plasma-sprayed Al_2O_3-CNT coatings in dry sliding condition against ZrO_2 pin at a normal load of 48 N (Ref 13). An improvement of 49 times in the sliding wear resistance of Al_2O_3-8 wt.% CNT coating was observed (Ref 13). This improvement was attributed to a uniform dispersion of nanotubes, CNT bridging between the splats, and enhanced densification by CNTs. In another study, tribological behavior of plasma-sprayed Al_2O_3-1.5 wt.% CNT coating was investigated at elevated temperature (~573, 873 K) against tungsten carbide (WC) ball as a counterpart at a normal load of 30 N (Ref 8). This coating was synthesized by plasma spraying using Al_2O_3 powder having chemical vapor-deposited (CVD) CNTs on the powder surface. The wear surface showed formation of tungsten oxide (WO_3)-rich protective layer because of tribochemical reaction with WC ball at elevated temperature

Anup Kumar Keshri and **Arvind Agarwal**, Plasma Forming Laboratory, Mechanical and Materials Engineering, Florida International University, 10555 West Flagler Street, EC 3464, Miami, FL 33174; **Anup Kumar Keshri** and **Arvind Agarwal**, High Temperature Tribology Laboratory, Mechanical and Materials Engineering, Florida International University, 10555 West Flagler Street, EC 3464, Miami, FL 33174; and **Anup Kumar Keshri**, Manufacturing Division, School of Mechanical and Building Sciences, Vellore Institute of Technology, Vellore, Tamilnadu 632014, India. Contact e-mail: agarwala@fiu.edu.

(Ref 8). Relative improvement in the wear resistance of Al_2O_3-1.5 wt.% CNT coating was found to be ~12% at room temperature, 56% at 573 K, and 82% at 873 K (Ref 8). Improved wear resistance of Al_2O_3-CNT coating was attributed to (i) large area coverage by protective film at the elevated temperature, (ii) higher hardness than Al_2O_3 coating, and (iii) CNT bridging between splats.

Though our previous studies provided an insight into the wear behavior of plasma-sprayed Al_2O_3-CNT coatings (Ref 8, 13), no information could be determined about tribological behavior in marine environment. To the best of our knowledge, no study has been reported in the literature on the tribological behavior of plasma-sprayed Al_2O_3-CNT coatings in sea water. In the present study, the tribological behavior of plasma-sprayed Al_2O_3-CNT coatings is investigated at room temperature (298 K), elevated temperature (873 K), and in sea water, using ball-on-disk tribometer against a Si_3N_4 ball. Hence, the novelty of this study is two-fold: (i) tribological behavior of Al_2O_3-CNT composite coatings in marine environment, and (ii) high-temperature wear behavior of Al_2O_3-CNT composite coatings at a higher CNT content of 4 and 8 wt.%. Our previous (Ref 8) high-temperature wear study of Al_2O_3-CNT composite was restricted to mere 1.5 wt.% CNTs, which is significantly lower than 4 and 8 wt.% CNTs adopted in the present study.

2. Experimental Procedure

2.1 Coating Synthesis

Three different spray-dried powders *viz.* Al_2O_3 (referred as A-SD), Al_2O_3-4 wt.% CNT (referred as A4C-SD), and Al_2O_3-8 wt.% CNT (referred as A8C-SD) were plasma sprayed using SG 100 gun (Praxair Surface Technology, Danbury, CT) on AISI 1020 steel substrate (100 mm × 19 mm × 3.2 mm) to synthesize Al_2O_3 and Al_2O_3-CNT coatings. Optimized plasma parameters to obtain high density coating were employed to synthesize the Al_2O_3 and Al_2O_3-CNT coatings and are listed in Table 1. The details of powder processing and optimization are published elsewhere (Ref 16).

2.2 Microstructural and Mechanical Characterization

A JEOL JSM 6330 F field emission scanning electron microscope (FE-SEM) was employed to investigate the microstructural and topographical features of the worn surface of plasma-sprayed Al_2O_3-CNT coatings. X-ray mapping was performed using a JEOL JSM 5910LV scanning electron microscope (SEM) operating at 15 kV with 16 frames in a matrix of 1024 × 800 pixels taking 50 μs per square pixel, each pixel being of dimensions 0.336 μm in the x and y equally. Micro-Raman spectroscopy (spatial resolution: 5 μm) was employed to study the CNT structure in Al_2O_3-CNT coatings before and after wear. A titanium (Ti)-sapphire crystal target with a laser wavelength of 785 nm was used, and the laser was produced using a source from Spectra Physics (Model 3900 S, CA, USA) with the detector (spectral resolution: 4 cm^{-1}) from Kaiser optical system, Inc. (MI, USA). The wear tracks of the Al_2O_3-CNT coatings after room temperature (298 K) and high-temperature testing (873 K) were characterized using Physical Electronics (PHI 5400) ESCA x-ray photoelectron spectroscopy (XPS). Nonmonochromatic x-ray radiation from Mg Kα source of 300 W was used for the analysis. Vickers microhardness tester (MHT Micro Photonics Inc., CA) at a load of 4 kg, and 30 seconds dwell time was applied to measure the microhardness of the coatings. Fracture toughness by indentation method was evaluated using Anstis equation (Ref 17).

2.3 Tribological Studies

Ball-on-disk tribometer (Nanovea, Micro Photonics Inc., CA, USA) having options of conducting wear experiments at high temperature and in lubricating media was employed to evaluate the wear resistance of the coatings. Wear tests were conducted at room temperature (298 K), elevated temperature (873 K), and in sea water. Sea water studies were conducted at room temperature (298 K). Sea water was prepared according to the ASTM1141-98 standard (Ref 18) as shown in Table 2.

Wear tests were carried out at 250 rpm (linear sliding velocity: 0.156 m/s) and at a normal load of 30 N with a stationary ball and the rotating sample. Each wear test was conducted for 60 min resulting in 15000 revolutions which correspond to 565 meters linear travel distance. A 3 mm-diameter silicon nitride (Si_3N_4) ball was employed to slide against the coating surface. The surface of the plasma-sprayed coatings was polished to an average roughness (R_a) value of ~1.0-2.5 μm. Surface roughness of the

Table 2 Chemical composition of sea water (Ref 18)

Compound	Concentration, g/L	Compound	Concentration, g/L
NaCl	24.530	KCl	0.695
Na_2SO_4	4.093	$NaHCO_3$	0.201
$MgCl_2$	5.212	KBr	0.101
$CaCl_2$	1.161	H_3BO_3	0.027
$SrCl_2$	0.025	NaF	0.003

Table 1 Plasma-spraying parameters for synthesizing A-SD, A4C-SD, and A8C-SD coatings

Current, A	Voltage, V	Primary gas, argon, slm	Secondary gas, helium, slm	Stand-off (mm) from the substrate	Powder feed rate, g/min	Substrate preheat temperature, K
850	40	56.6	59.5	75	3	453

polished coatings was measured using surface roughness analyzer TR 200 (Micro Photonics Inc., CA). The worn surface profile was investigated using a non-contact 3D optical profilometer PS50 (Nanovea, CA, USA). The resultant profile images were processed using image processing software SPIP™ (Image Metrology A/S, Horsholm, Denmark) to calculate the wear volume. Depth profiles were taken along lines drawn parallel as well as perpendicular to the wear track. Three wear tests were conducted for each condition to evaluate the consistency of the wear volume loss and coefficient of friction (COF). The frictional force between the ball and the coating surface was measured by the linear variable differential transformer (LVDT) sensor. The data were acquired at a rate of 1000 data points per minute.

3. Results and Discussion

3.1 Plasma-sprayed Al_2O_3-CNT Coatings

A brief background of the powder processing and the coating synthesis are described here for the benefit of readers and sake of completeness. The details are published elsewhere (Ref 16). Fine Al_2O_3 powder (150 nm) was reinforced with multiwall CNTs of varying content (0, 4, and 8 wt.%), by spray-drying technique. The spray-dried agglomerates contain high amounts of porosity (~30-40%), but this improves flowability of the powder because of the spherical shape and reduced interparticle friction between nanoparticles. CNTs were uniformly dispersed on the surface of agglomerate which is critical for an improvement in the mechanical and tribological properties. A-SD, A4C-SD, and A8C-SD composite coatings were synthesized by plasma spraying of spray-dried Al_2O_3, Al_2O_3-4 wt.% CNT, and Al_2O_3-8 wt.% CNT powders, respectively. Coatings have a uniform thickness of 400 μm with a theoretical density of ~96% for A-SD coating and ~96.5 and ~97% for A4C-SD and A8C-SD coatings, respectively, as measured by the water immersion technique (Ref 16). The slightly higher density in CNT containing coatings is attributed to the uniform dispersion of nanotubes in the agglomerates, which causes uniform melting and intersplat void filling (Ref 16).

Figure 1(a) and (b) shows the fracture surface of A4C-SD and A8C-SD coatings, respectively. CNTs are dispersed within Al_2O_3 splats. Table 3 shows the microhardness and fracture toughness of A-SD, A4C-SD, and A8C-SD coatings. Owing to limitations associated with measurement of true fracture toughness of ceramics by indentation and SEVNB (Single edge V-notched beam) methods (Ref 19-21), we have emphasized on relative improvement in the fracture toughness in Table 3. Improvement in the microhardness of CNT-reinforced coatings is attributed to the enhanced indentation resistance due to CNTs. Significant improvement in the fracture toughness of CNT-reinforced coatings is attributed to the combined effect of lower porosity and the distributed CNTs in the Al_2O_3 matrix, which promotes toughening mechanisms. SEM investigation inside the indentation crack elucidates the toughening mechanisms offered by CNTs. Figure 2(a) shows the high magnification SEM image of Vickers indent at 4 kg load showing the fine radial crack in A8C-SD coating. Figure 2(b) display high magnification SEM images within the crack in A8C-SD coating. CNT bridging between the splats resists the crack widening and propagation, and hence, contributes toward the toughening. Uniformly dispersed CNTs in Al_2O_3 matrix provide multiple sites for anchoring and bridging the splats resulting in uniform toughening. Crack deflection

Table 3 Vickers microhardness and fracture toughness of A-SD, A4C-SD, and A8C-SD coatings

	Hardness, VHN	Fracture Toughness, MPa $m^{1/2}$	Relative improvement % in fracture toughness (compared to A-SD coating)
A-SD	1498 ± 62	0.93 ± 016	…
A4C-SD	1606 ± 53	1.75 ± 0.25	88
A8C-SD	1670 ± 41	4.09 ± 0.58	339

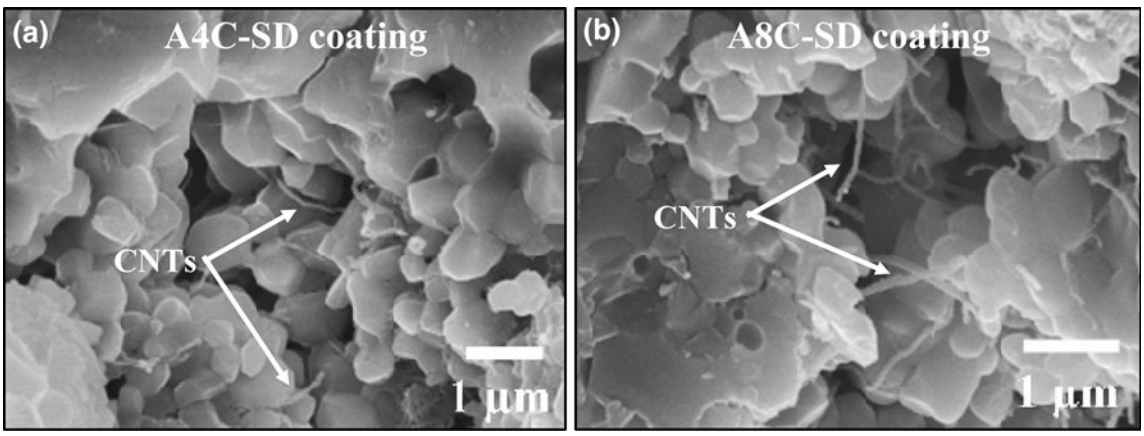

Fig. 1 SEM images of fracture surfaces of (a) A4C-SD coating and (b) A8C-SD coating showing CNTs in the Al_2O_3 matrix

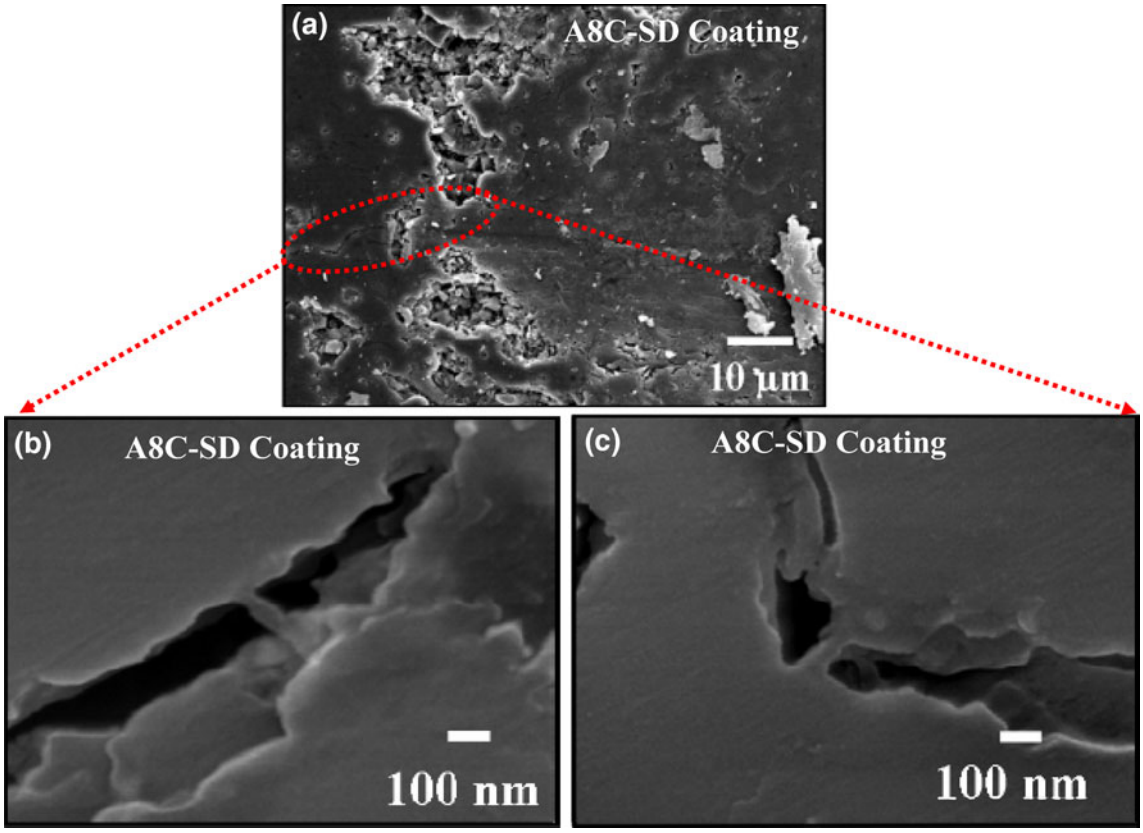

Fig. 2 (a) High magnification SEM image of Vickers indent at 4 kg load for A8C-SD coating showing fine radial crack. (b) High magnification SEM image within the crack for A8C-SD coating showing CNT bridging inside the crack. (c) High magnification SEM image within the crack for A8C-SD coating showing crack deflections at Al_2O_3-CNT interface

at CNT/Al_2O_3 interface is also observed in the A8C-SD coating. Figure 2(c) shows that crack deflects to another direction after it interacts with CNT bridge. Such deflection results in the dissipation of crack energy resulting in improved fracture toughness.

3.2 Wear Behavior at Room and High Temperatures

Figure 3 shows the wear volume loss as a function of temperature at a normal load of 30 N for A-SD, A4C-SD, and A8C-SD coatings. Wear volume loss of each coating in sea water is also shown in Fig. 3 which will be discussed later in section 3.3. Percentage value shown in Fig. 3 is the relative improvement in the wear resistance of that coating relative to A-SD coating. Volume loss increases with the temperature for all coatings, while it decreases with an increasing CNT content when sliding against Si_3N_4 counter body. The difference in the volume loss due to wear is clearly shown in 3D optical profiles in Fig. 4. Figure 4(a) and (b) shows the 3D optical profiles of wear tracks of A-SD and A8C-SD coatings, respectively, at 298 K, while Fig. 4(c) and (d) shows the 3D optical profile images of wear track of A-SD and A8C-SD coatings, respectively, at 873 K. The wear profile for A4C-SD (i.e., intermediate CNT content) is not shown here for the sake of brevity. Similarly, wear track profiles of A-SD and A8C-SD

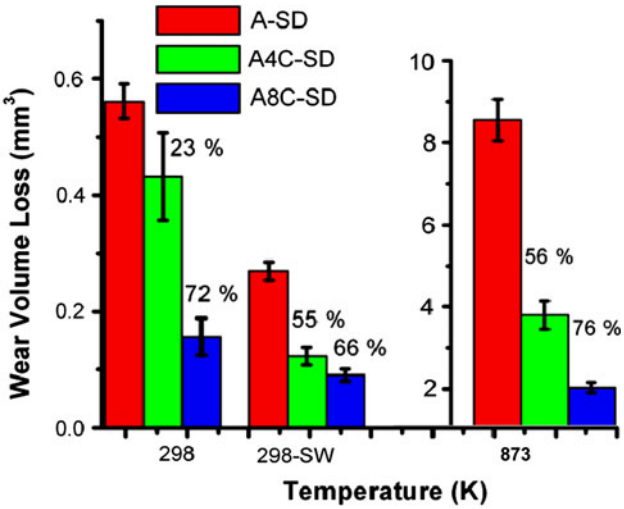

Fig. 3 Wear volume loss of A-SD, A4C-SD, and A8C-SD coatings at room temperature (298 K), sea water (298-SW), and at 873 K. Percentage value shown above the bar is the relative improvement in the wear resistance of the that coating relative to Al_2O_3 (A-SD) coating

coatings in sea water are shown in Fig. 4(e) and (f), respectively. Inset image represents the depth and width of the corresponding wear track.

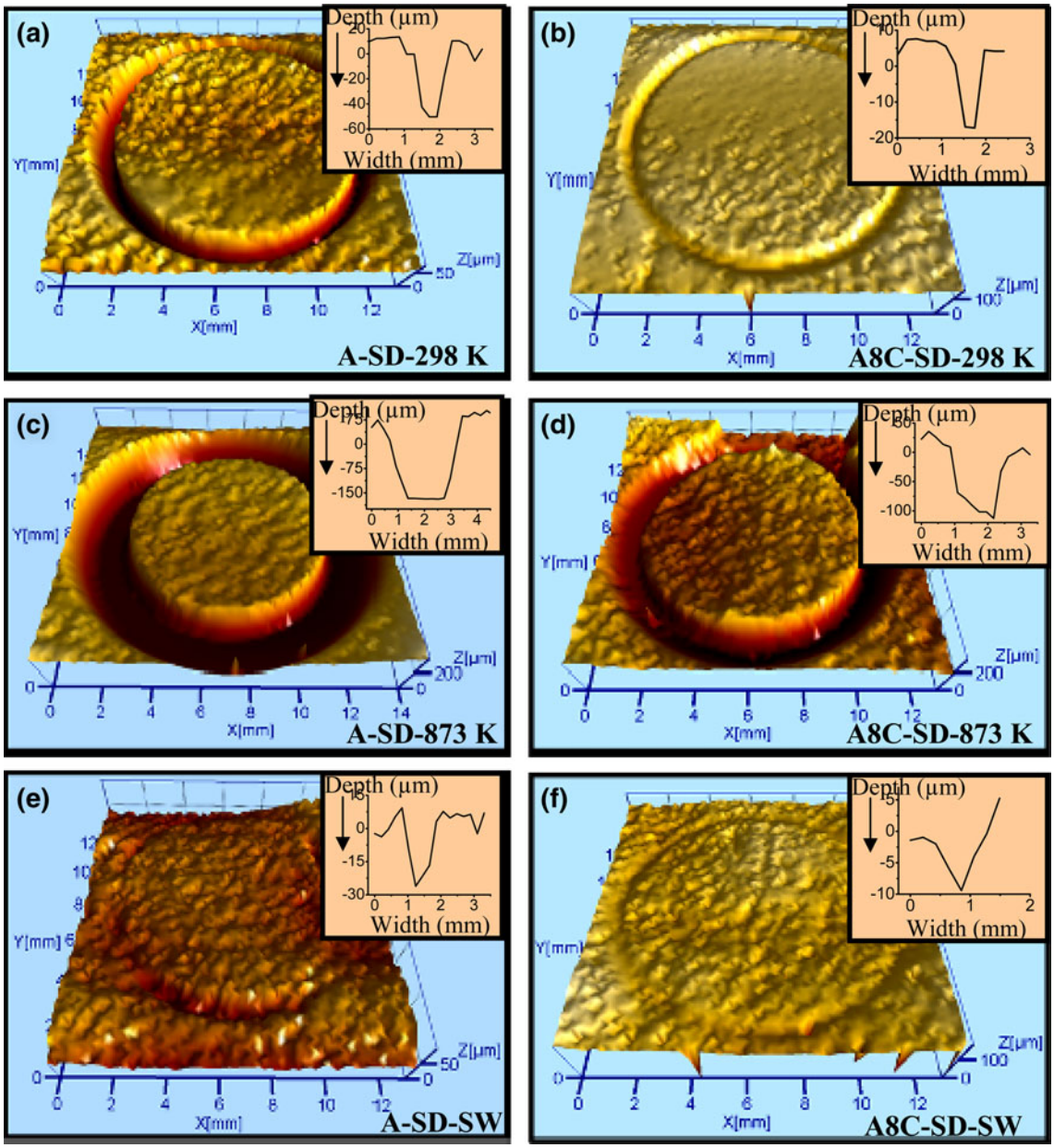

Fig. 4 3D optical profiles of worn surface of (a, b) A-SD and A8C-SD coatings at 298 K, (c, d) A-SD and A8C-SD coatings at 873 K, and (e, f) A-SD and A8C-SD coating in sea water. Inset image shows the depth of the wear track after the linear sliding distance of ~565 m at normal load of 30 N

Table 4 Wear depths, wear volume losses, and coefficients of friction for A-SD, A4C-SD, and A8C-SD coatings at 298 K, 873 K, and in sea water

	Wear depth, μm			Wear volume loss, mm^3			Coefficient of friction (COF)		
	298 K	873 K	Sea water	298 K	873 K	Sea water	298 K	873 K	Sea water
A-SD	52	180	22	0.56	8.54	0.27	0.71	0.82	0.59
A4C-SD	38	135	14	0.43	3.79	0.12	0.67	0.83	0.57
A8C-SD	17	105	8	0.15	2.03	0.09	0.65	0.83	0.55

Wear depths and wear volume losses for A-SD, A4C-SD, and A8C-SD coatings at 298 K, 873 K, and at sea water, are calculated from the wear profiles and are tabulated in Table 4. COF is also listed in Table 4, which will be discussed later in section 3.4. The highest wear depth and wear volume loss were observed for all coatings

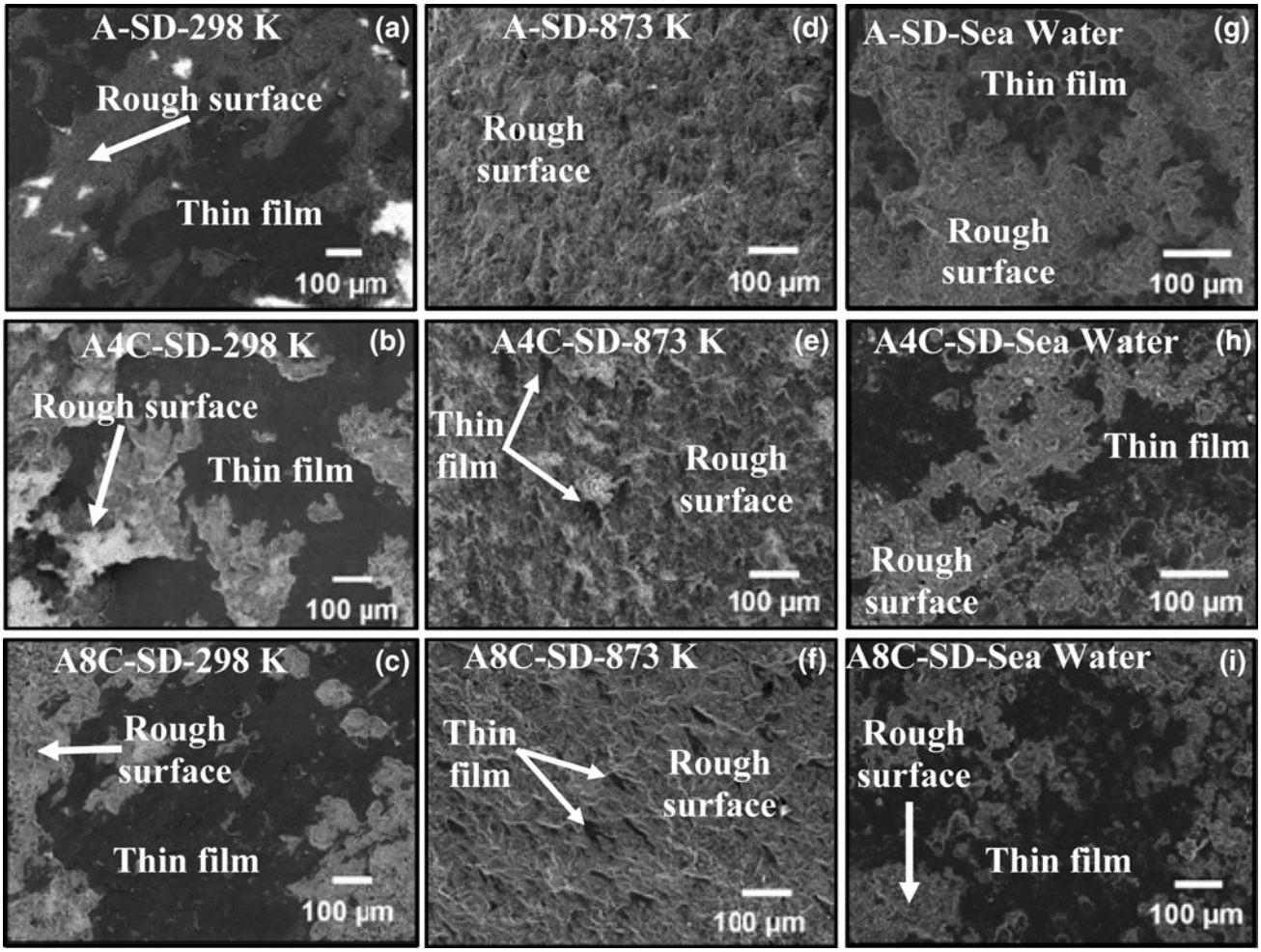

Fig. 5 Wear surface topography after the linear sliding distance of ~565 m and at normal load of 30 N for (a-c) A-SD, A4C-SD, and A8C-SD coatings, respectively, at 298 K, (d-f) A-SD, A4C-SD, and A8C-SD coating respectively at 873 K, and (g-i) A-SD, A4C-SD, and A8C-SD coating respectively in sea water

at 873 K, while the lowest wear was observed in sea water. The reinforcement effect of CNTs is clearly highlighted in Fig. 4 and Table 4, which reveals the lower wear depth and volume for CNT-reinforced Al_2O_3 coatings.

In order to understand the wear mechanism at different conditions, wear surfaces were observed under FE-SEM as shown in Fig. 5. Wear surface of coatings in sea water are also shown in Fig. 5. Figure 5(a)-(c) shows the SEM micrographs of wear surfaces of A-SD, A4C-SD, and A8C-SD coatings at 298 K, respectively. Similarly, Fig. 5(d)-(f) represents the SEM micrographs of wear surfaces of A-SD, A4C-SD, and A8C-SD coatings at 873 K, respectively. Wear surfaces of all the coatings at 298 K show bimodal characteristic of the *rough* and *smooth* surfaces. Wear surfaces of all the coatings at 873 K shows highly rough surface with only traces of dispersed smooth regions. Rough surface indicates the phenomena of severe wear whereas smooth region is due to thin film formation often due to a tribochemical reaction. Formation of a smooth, thin protective layer as a result of tribochemical reaction can reduce the wear of coating surface against sliding (Ref 9, 22, 23). The percentage of smooth area covered indicating thin film on the worn surface of A-SD, A4C-SD, and A8C-SD coatings at 298 and 873 K was measured from several locations on the wear track images using Image J software (http://rsbweb.nih.gov/ij/index.html). Table 5 shows the fraction of the area coverage of the smooth thin film on the wear track of coatings at 298 and 873 K. Smooth thin film was also observed in sea water wear condition (Fig. 5). Table 5

Table 5 Area fraction of thin film on the wear surface of A-SD, A4C-SD, and A8C-SD coatings at 298 K, 873 K and in sea water

	Room temperature (298 K)	High temperature (873 K)	Sea water
A-SD	0.63	Not observed	0.42
A4C-SD	0.69	0.08	0.55
A8C-SD	0.76	0.11	0.63

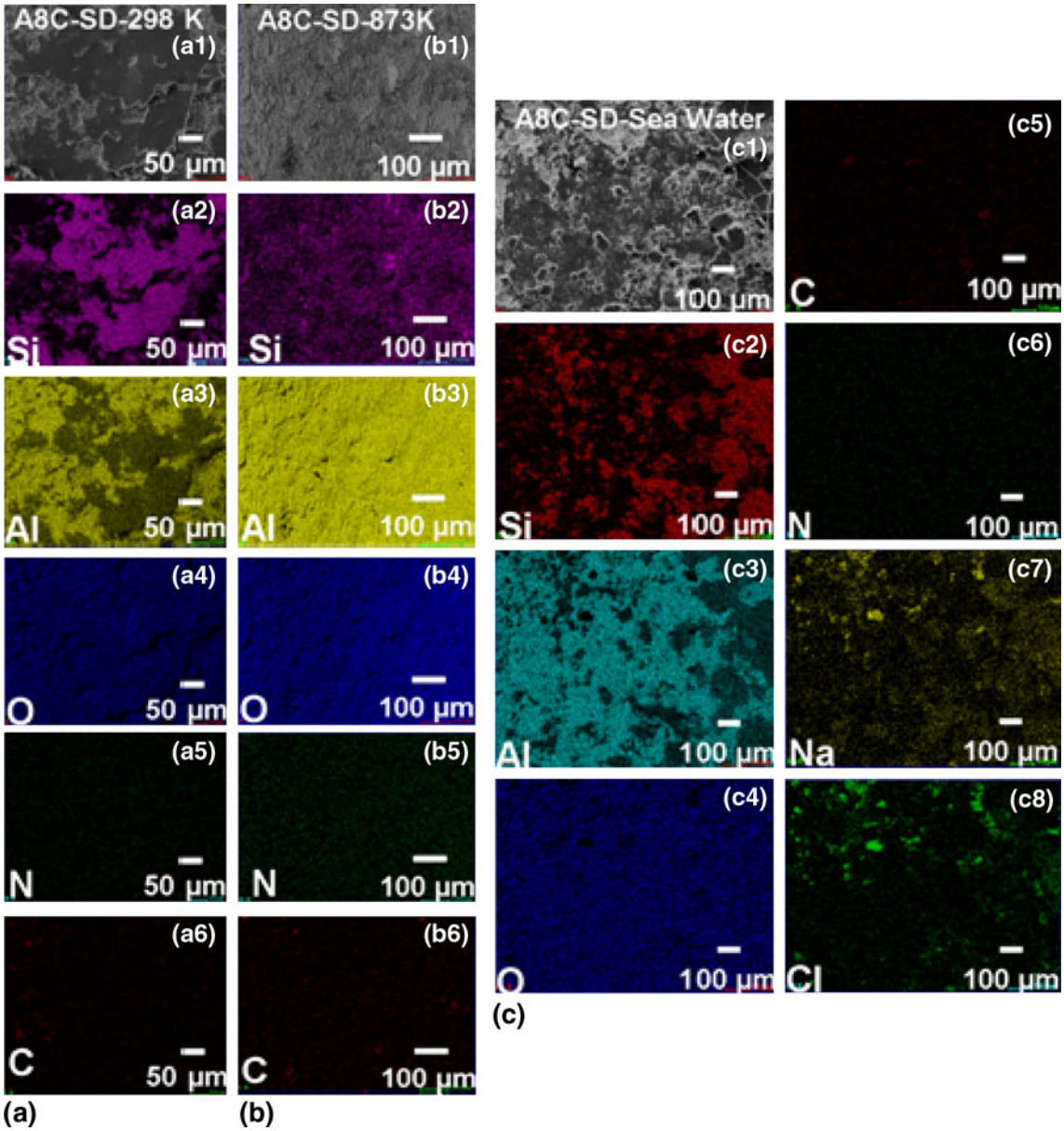

Fig. 6 X-ray maps of wear track of (a) A8C-SD at 298 K, (b) A8C-SD at 873 K, and (c) A8C-SD coating in sea water. a1, b1, and c1 are the backscattered images of wear tracks of A8C-SD coating at 298 K, 873 K, and in sea water, respectively. a2-a6, and b2-b6 show the distributions of silicon, aluminum, oxygen, nitrogen, and carbon, respectively, while c2-c8 shows the distribution of silicon, aluminum, oxygen, carbon, nitrogen, sodium, and chlorine, respectively

clearly indicates the higher transfer of smooth thin film in the case of coatings at 298 K and the lowest at 873 K.

Distribution of smooth thin film has also been observed by performing elemental x-ray mapping of the wear track. Figure 6 shows the elemental x-ray mapping of the wear surfaces of A8C-SD coating at 298 K, 873 K and in sea water. Figure 6(a1), (b1), and (c1) shows the back-scattered images of wear tracks of A8C-SD coating at 298 K, 873 K and in sea water, respectively. Figure 6(a2-a6) and (b2-b6) shows the distribution of silicon, aluminum, oxygen, nitrogen and carbon, respectively in the worn surface of A8C-SD coating at 298 and 873 K, respectively. X-ray map confirms the presence of silicon, nitrogen in the wear surface which is as results of tribochemical reaction with the Si_3N_4 ball. Si_3N_4 ball oxidizes in the presence of moisture and forms a protective film on the wear surface of coatings as a result of tribochemical reaction (Ref 9, 22, 24). High-temperature oxidation reaction of Si_3N_4 in the presence of moisture was analyzed with the help of FactSage thermochemistry software (Ref 25). Equations 1-3 show oxidation reactions from 298 to 1173 K and associated change in the Gibbs free energy. Equation 1 indicates the formation of crystalline SiO_2 as the reaction product at 298 K which changes to amorphous hydrated SiO_2 at 873 K.

Increasingly negative Gibbs free energy with the increasing temperature confirms thermodynamic stability of amorphous hydrated SiO_2 formation at higher temperature (873 K).

$$\text{At } 298\,\text{K:}\quad Si_3N_4 + 75H_2O + 1000O_2 = 997O_2 + 3SiO_2 + 71H_2O + 2N_2, \quad \Delta G = -9.05 \times 10^7\,\text{J} \qquad \text{(Eq 1)}$$

$$\text{At } 873\,\text{K:}\quad Si_3N_4 + 75H_2O + 1000O_2 = 996O_2 + 3SiO_2 \cdot nH_2O(\text{amorphous}) + 75H_2O + 2N_2, \quad \Delta G = -2.36 \times 10^8\,\text{J} \qquad \text{(Eq 2)}$$

$$\text{At } 1173\,\text{K:}\quad Si_3N_4 + 75H_2O + 1000O_2 = 996O_2 + 3SiO_2 \cdot nH_2O(\text{amorphous}) + 75H_2O + 2N_2, \quad \Delta G = -3.19 \times 10^8\,\text{J} \qquad \text{(Eq 3)}$$

XPS analysis of the wear surface of A8C-SD coating at 298 K and 873 K in Fig. 7 shows the single major peak at 103.5 eV corresponding to SiO_2. This is in good agreement with the reported literature value where the single peak with $E_b = 103.3$ eV corresponds to Si 2p bond in SiO_2 (Ref 26, 27). It should be noted that Eq 2 shows the formation of amorphous hydrated SiO_2 as reaction product at 873 K, while XPS shows the presence of crystalline SiO_2. This is attributed to the transformation of amorphous hydrated SiO_2 to crystalline SiO_2 below ~823 K (Ref 25). It must be recalled that the most of the room temperature wear surfaces of coatings were covered with protective tribochemical SiO_2 film that reduced the wear volume loss. However, the absorption tendency of moisture decreases at higher temperature, and hence results in a reduced fraction of protective film formation. This is observed in Fig. 5(d)-(f), which shows only traces of smooth region which is indicative of protective SiO_2 film.

In our previous study on tribological behavior of Al_2O_3-1.5 wt.% CNT coating at elevated temperature (Ref 8), wear resistance of the coatings was found to increase at 873 K when sliding against tungsten carbide (WC) ball. This was attributed to the presence of relatively larger amounts of tungsten oxide (WO_3) protective layer on the wear track as a result of tribochemical reaction (Ref 8). This shows the strong effect of counterpart on tribological behavior of Al_2O_3 coating, especially at elevated temperatures. Sliding wear against WC ball showed protective layer formation at elevated temperature (Ref 8), whereas sliding against Si_3N_4 ball shows protective layer formation at room temperature (Ref 9). Si_3N_4 ball in post-wear condition was examined to further understand the wear mechanism. It was expected that there will be more transferred layer from the coating to Si_3N_4 ball surface in severe wear conditions. Figure 8(a) shows unworn surface of the Si_3N_4 ball whereas Fig. 8(b) and (c) shows the worn surfaces of Si_3N_4 ball after the wear at 298 and 873 K, respectively. Unworn Si_3N_4 ball shows a smoother surface, whereas rough surface is observed for 298 and 873 K. From Fig. 8(b) and (c), it can be concluded that the wear surface of the ball at 873 K has higher fraction of the transfer layer from the coating. Composition of the transfer layer has been identified by performing EDS and x-ray mapping on the worn surface of Si_3N_4 ball. EDS spectrum of the worn ball in Fig. 8(d) shows high intensity peak for aluminum. Table 6 presents the quantitative EDS analysis of elements, which shows high weight percentages of aluminum and oxygen on the worn ball surface, indicating higher amount of transfer layer from the wear track to ball as a result of severe wear of Al_2O_3-based coatings. The transfer layer on Si_3N_4 ball also shows carbon peak, which originates from the wear of A8C-SD coating.

Higher transfer of layers from the A8C-SD coating to ball suggest severe wear of the coating. Severe wear of the coating at ~873 K also has an adverse effect on the toughening mechanism offered by CNTs. Owing to severe wear of coating, some of the reinforced CNTs might get exposed to elevated temperature (873 K) resulting in their oxidation. Osswald et al. (Ref 28) monitored the oxidation of CNTs by Raman spectroscopy and concluded that

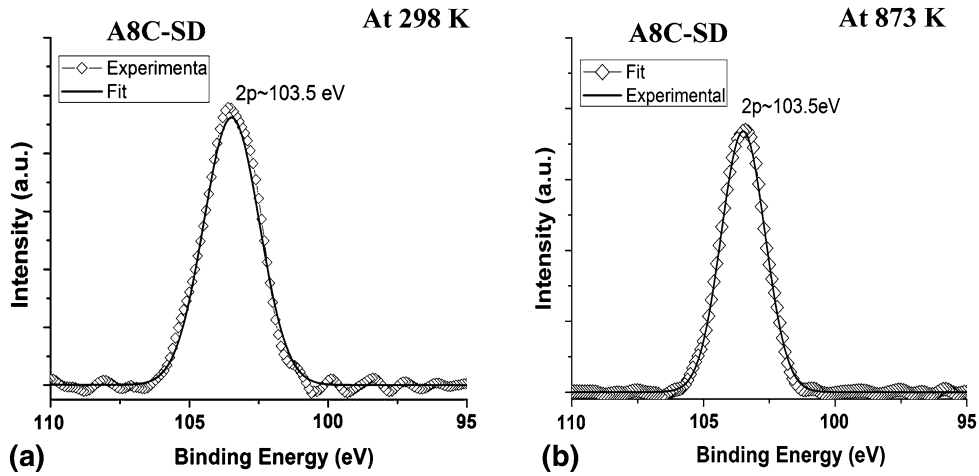

Fig. 7 XPS spectra collected from wear track of A-8CSD coating (a) at 298 K and (b) at 873 K. Both the spectra show the major peak of Si 2p near ~103.5 eV confirming the presence of SiO_2 layer on the surface of wear track

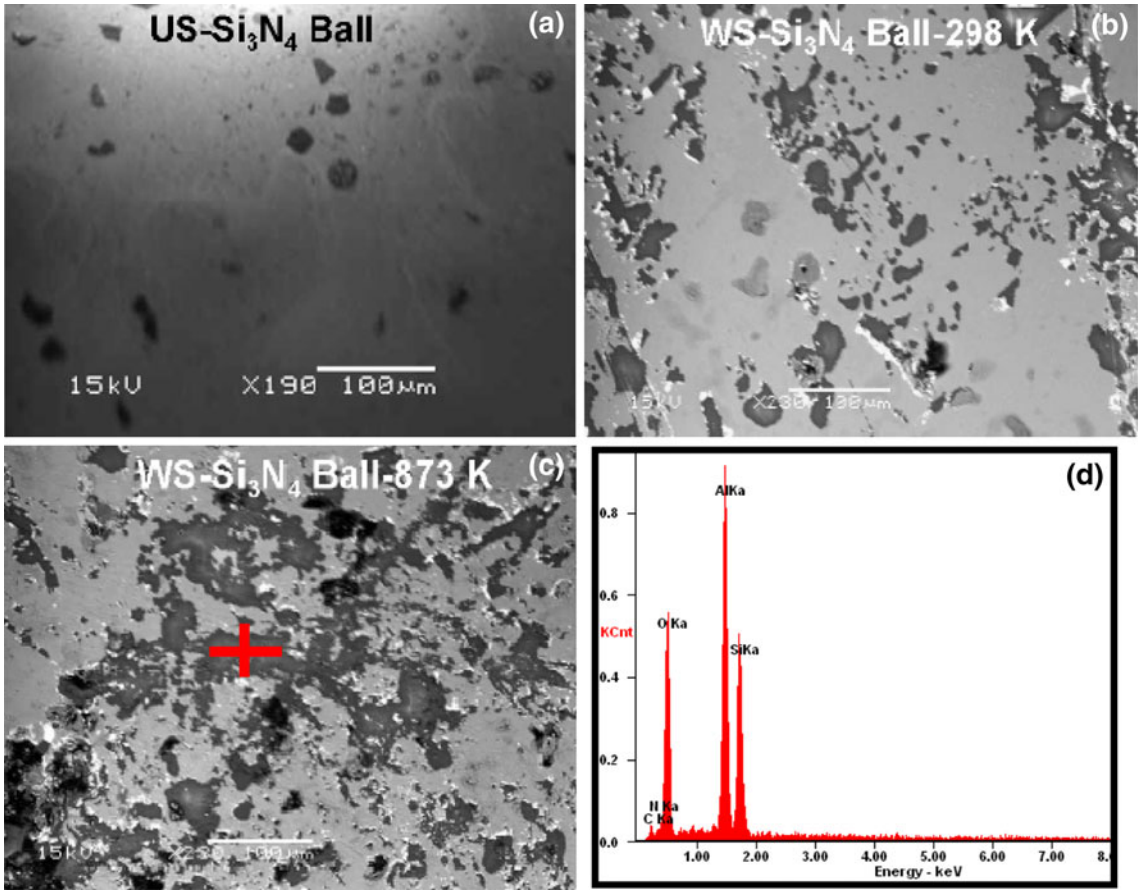

Fig. 8 (a) Unworn surface (US) of Si_3N_4 ball, (b) worn surface (WS) of Si_3N_4 ball after the wear test at ~298 K, (c) Worn surface (WS) of Si_3N_4 ball after the wear test at ~873 K, and (d) EDS spectra collected from the worn surface of ball. Wear surface of Si_3N_4 ball are shown after conducting experiments against A8C-SD coating

Table 6 Quantitative EDS analysis obtained from the worn surface of Si_3N_4 ball after conducting experiments against A8C-SD coating at 873 K

Element	wt.%	at.%
CK	4.81	7.81
NK	8.59	11.97
OK	36.62	44.65
AlK	**29.66**	**21.44**
SiK	20.33	14.12

oxidation of CNT occurs above 440 °C with a severe rate at 550-600 °C. Li et al. (Ref 29) also concluded that oxidation of CNTs occurs in the temperature range of 480-750 °C in air. Oxidation of CNT might lead to defect generation in the tubular structure, which has been studied by collecting Raman spectra from the wear tracks of A4C-SD and A8C-SD coatings at 873 K. Figure 9(a) and (b) shows the Raman spectra for unworn and worn surfaces of A4C-SD and A8C-SD coatings, respectively, at 298 K, 873 K, and in sea water. Positions of D and G peaks and I_D/I_G ratios in Table 7 were calculated from the Raman spectra. I_D/I_G ratio was slightly higher for the wear surfaces of A4C-SD and A8C-SD coatings at 873 K as compared with unworn coating. Increased I_D/I_G ratio is the indication of more defects in the CNTs in the worn surfaces of A4C-SD and A8C-SD coatings which might be due to oxidation of CNTs at elevated temperature (873 K). This could degrade the toughening effect of CNTs to some extent and lower the wear resistance as observed in Fig. 3. In our previous study on wear of Al_2O_3-1.5 wt.% CNT coatings at 873 K (Ref 8), lower I_D/I_G ratio was observed from the worn surface at 873 K against WC ball, which is contrary to the present study. Such behavior was attributed to the formation of high fraction of protective WO_3 film at high temperature which not only prevents oxidation of CNTs, but also maintains the toughening caused by CNTs (Ref 8).

Figure 3 also shows that wear resistance improves with the increasing CNT content. Relative increase in the wear resistance of CNT-reinforced coating is attributed to the higher fracture toughness of CNT-reinforced coatings. Reinforcement by 4 and 8 wt.% of CNTs showed ~88 and ~338% improvement, respectively, in the fracture toughness of Al_2O_3 coating (as shown in Table 3). Evans and Marshall equation confirms that higher fracture toughness results in higher wear resistance of the ceramic (Ref 30). Figure 10(a) and (b) shows the CNT bridging between the

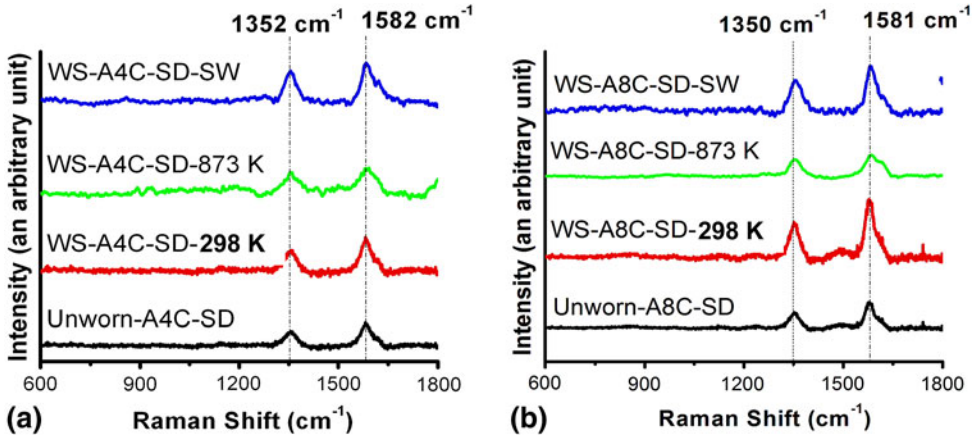

Fig. 9 Raman spectra of unworn (US) and worn surfaces (WS) of (a) A4C-SD, and (b) A8C-SD coatings at room temperature, 873 K, and at sea water

Table 7 Ratios of intensity of D and G peaks obtained from Raman spectroscopy of unworn surfaces (US) and worn surfaces (WS) of A4C-SD and A8C-SD coatings at room temperature, 873 K, and at sea water

	A4C-SD coating			A8C-SD coating		
	Position of D peaks	Position of G peaks	I_D/I_G	Position of D peaks	Position of G peaks	I_D/I_G
Unworn surface	1356	1582	0.84	1356	1582	0.93
Worn surface at RT	1361	1588	0.76	1362	1584	0.73
Worn surface at 873 K	1356	1583	0.96	1353	1586	0.98
Worn surface at SW	1356	1585	0.80	1357	1581	0.67

splats in wear tracks of A4C-SD and A8C-SD coatings at 298 K. Figure 10(c, d) and (e, f) shows CNT bridging between the splats in wear tracks of A4C-SD and A8C-SD coatings at 873 K and in sea water respectively. CNT bridging reduces the degree of material removal by resisting the crack propagation and improving the toughening. It is true that at higher temperature, oxidation of CNTs may degrade the toughening effect to some extent and lower the wear resistance. Our results indicate that CNT-reinforced coatings displayed improved wear resistance even at higher temperature, though wear resistance was more significant at room temperature.

3.3 Wear Behavior of Coatings in Sea Water

Figure 3 also shows the wear volume loss of A-SD, A4C-SD, and A8C-SD coatings in sea water. All coatings exhibit lowest wear volume loss in sea water as compared to dry sliding at room and elevated temperature. In addition, the wear volume decreased with an increasing CNT content in sea water environment. Figure 4(e) and (f) shows the 3D optical profiles of wear track of A-SD and A8C-SD coatings in sea water. Inset shows the depth of the wear track clearly highlighting the lowest wear volume loss and wear depth in sea water as compared to 298 and 873 K. Figure 5(g)-(i) shows the worn surfaces of A-SD, A4C-SD, and A8C-SD coatings in sea water. Regions of high roughness and smooth thin film formation were observed in all coatings. Figure 6 shows the elemental x-ray mapping of the wear surface in sea water. Figure 6(c1) is the backscattered image of wear track of A8C-SD coating. Figure 6(c2)-(c7) shows the distribution of silicon, aluminum, oxygen, nitrogen, carbon, sodium, and chlorine respectively. X-ray maps confirm the presence of silicon, and nitrogen similar to dry sliding wear. This is attributed to the tribochemical reaction with the Si_3N_4 ball and formation of a thin protective SiO_2 film. The area fraction of the protective film on the worn surface of the coatings in sea water is relatively lower as compared with dry sliding (Table 5). This is attributed to a higher probability of dissolution of the transfer layer in the sea water as elucidated in Fig. 11.

It is noteworthy that even though sea water wear results in lower area fraction of the protective film, it exhibits the highest wear resistance. This is attributed to the following reasons: (i) antifriction natures of Cl^-, Mg^{2+}, and Ca^{2+} ions in sea water results in relatively lower wear debris generation (Ref 17), (ii) entrapped wear debris in sea water acts as rolling points resulting in smoother wear process, and (iii) dense microstructure (~96-97.5%) of the coating does not allow significant penetration of Cl^- ions to cause corrosion. It is also possible that total wear time (60 min) was not large enough to cause corrosion-enhanced wear of the coatings. Yan et al. (Ref 10) investigated the corrosion behavior of Al_2O_3-based ceramic coating in dilute HCl solution and showed that significant weight loss in the coating was found after 5 h of corrosion time in 1 N HCl solution (Ref 10). The improved wear resistance in sea

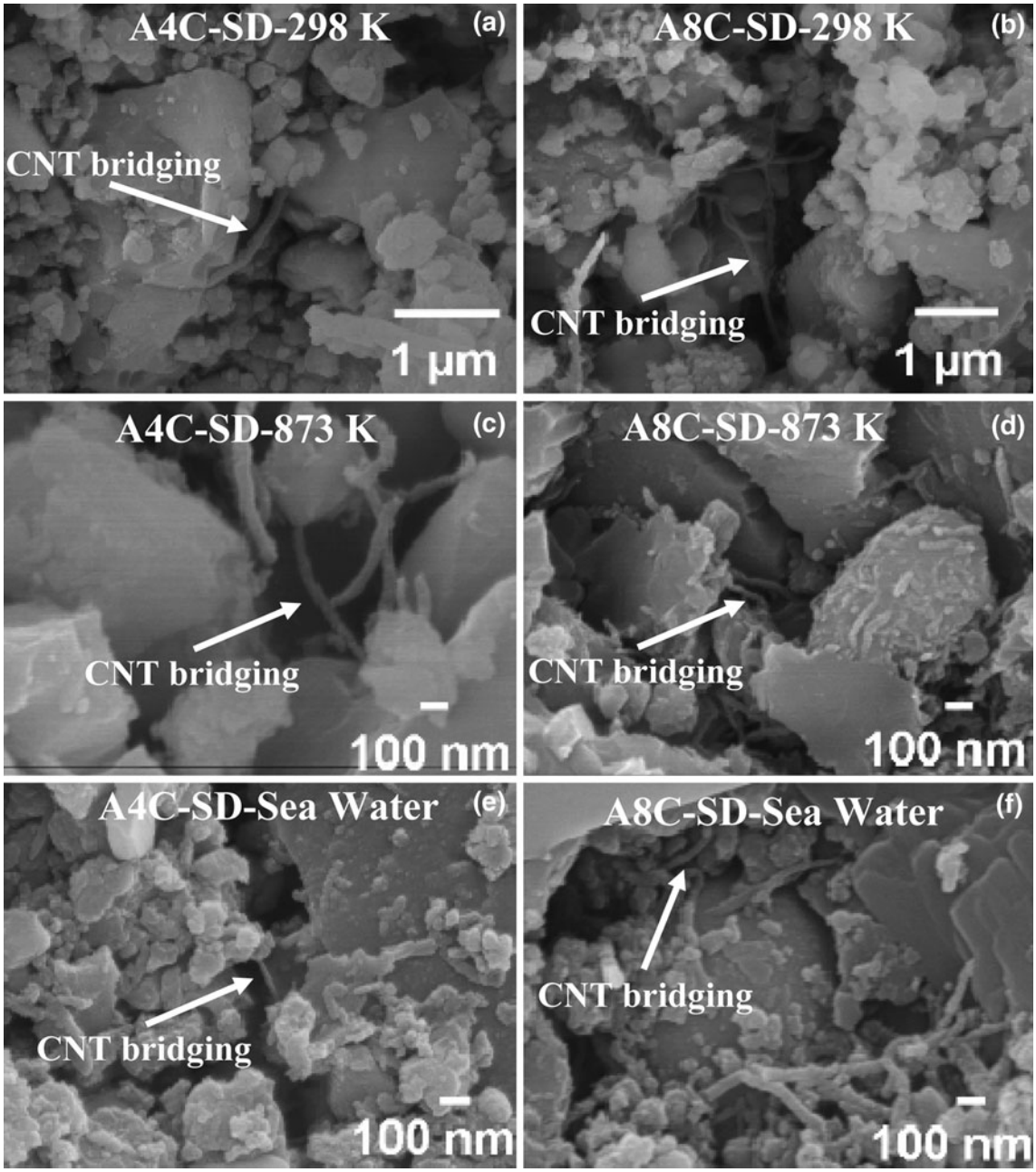

Fig. 10 High magnification images of wear surface (a, b) A4C-SD and A8C-SD coatings at 298 K; (c, d) A4C-SD and A8C-SD coatings at 873 K; and (e, f) A4C-SD and A8C-SD coatings in sea water, showing the CNT bridging between the splats

water for higher CNT content coatings is due to higher fracture toughness caused by CNT reinforcement. Figure 10(e) and (f) shows CNT bridging between the splats in the wear tracks of A4C-SD and A8C-SD coatings in sea water. CNT bridging reduces the degree of material removal by resisting the crack propagation.

3.4 Friction Behavior of Coatings

Figure 12 shows the dynamic COFs for A-SD, A4C-SD, and A8C-SD coatings at 298 K, 873 K, and in sea water during the entire travel distance of 565 m. An average COF value is shown in Table 4 for all the three coatings at different temperatures and in sea water. The average value of COF is obtained from the best-fit line in the steady region of the curve. The lowest COF was found for all the coatings in seawater. This was due to the anti-friction effects of sea water and the entrapped wear debris, which act as rolling points resulting in lower COF values in sea water. The highest COF was observed for all the coatings at 873 K, which is attributed to the presence of negligible amount of protective film on the wear track.

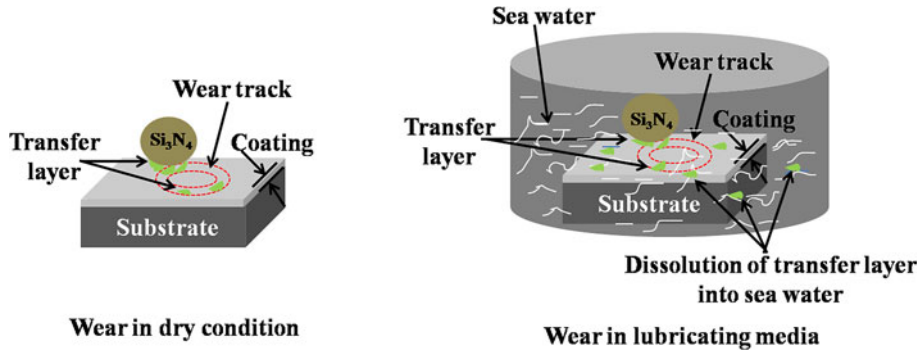

Fig. 11 Schematic of wear process in dry and sea water environment

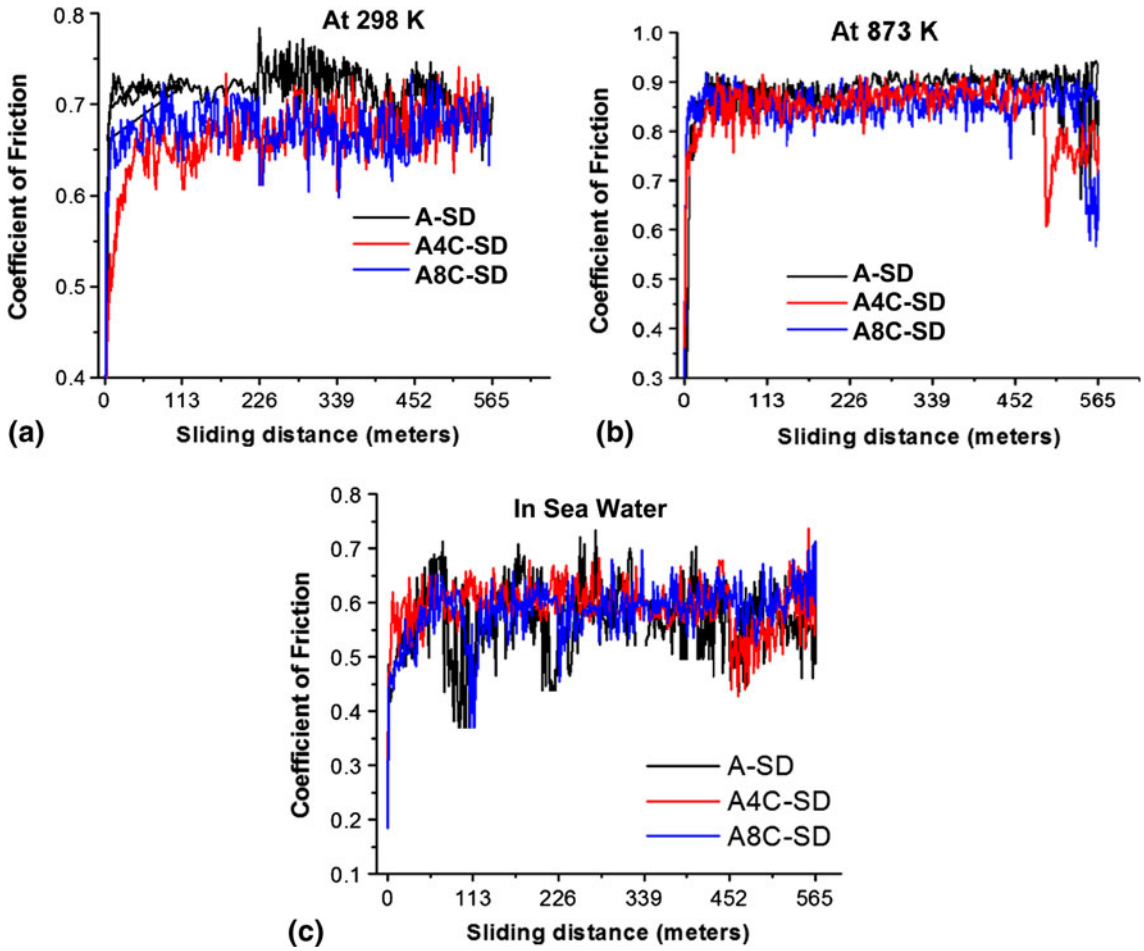

Fig. 12 Coefficient of friction (COF) with sliding distance at normal load of 30 N for wear track of coating (a) at 298 K, (b) at 873 K, and (c) in sea water

Hence, large amounts of wear debris generated in the wear track results in higher asperities and the highest COF.

It is also observed that CNT-reinforced coatings have slightly lower COFs at 298 K and in sea water, while COF is almost similar at 873 K. This behavior could be explained in terms of graphitization of CNTs due to wear, which can be examined from I_D/I_G ratio from the Raman spectra of the wear track. Table 7 shows the I_D/I_G ratios for unworn and worn surfaces of all the coatings. It is observed that I_D/I_G ratio from the worn surfaces of A4C-SD and A8C-SD coatings is lower as compared with unworn surfaces at room temperature and sea water. A lower I_D/I_G value indicates higher degree of graphitization

in the wear surface, which might be due to exposed graphene layer of CNTs by continuous abrading of the wear surface. Hence, a relatively lower COF was observed for CNT-reinforced coatings. However, in the case of wear at 873 K, CNT-reinforced coatings showed almost similar COF with A-SD coating (Table 4). I_D/I_G ratio from the worn surfaces of A4C-SD and A8C-SD coatings is higher at 873 K as compared with unworn surface, which indicates higher defect density caused by oxidation of CNTs at elevated temperature. Hence, no contribution from CNTs was observed in lowering COF in A4C-SD and A8C-SD coatings at 873 K.

4. Conclusions

Tribological behavior of plasma-sprayed Al_2O_3 and Al_2O_3-CNT coatings was evaluated at room temperature (298 K), elevated temperature (873 K), and in sea water. The wear surface shows formation of SiO_2-rich protective layer because of tribochemical reaction with Si_3N_4 ball at room temperature and in sea water. With increasing temperature, wear volume loss increased for A-SD, A4C-SD, and A8C-SD coatings. This was mainly due to negligible presence of the SiO_2 protective layer on the wear track at elevated temperature. Addition of 8 wt.% of CNT increases the wear resistance of Al_2O_3 (A-SD) coating by 72% at room temperature, ~76% at 873 K, and ~66% in sea water. Higher wear resistance of CNT-reinforced coating was attributed to (i) higher fraction of SiO_2 protective film on the wear surface at room temperature and sea water, (ii) higher fracture toughness of CNT-reinforced coating, and (iii) antifriction effect of sea water. Average COF was the lowest in sea water and the highest at 873 K.

Acknowledgments

The authors acknowledge the financial support received from the Office of Naval Research (N00014-08-1-0494). AKK acknowledges support from the Dissertation Year Fellowship by the University Graduate School of Florida International University (FIU). The authors are also grateful to the Center for the Study of Matter at Extreme Conditions (CeSMEC), FIU for allowing them to carry out Raman spectroscopy, and the Advanced Materials Engineering Research Institute (AMERI), FIU to avail the scanning electron microscopy facility.

References

1. K. Balani and A. Agarwal, Process Map for Plasma Sprayed Aluminum Oxide-Carbon Nanotube Nanocomposite Coatings, *Surf. Coat. Technol.*, 2008, **202**, p 4270-4277
2. E.H. Jordan and M. Gell, Nano Crystalline Ceramic and Ceramic Coatings Made by Conventional and Solution Plasma Spray, *Nanomaterials Technology for Military Vehicle Structural Applications*, RTO-MP-AVT-122, 3-4 October, 2005
3. G.R. Karagedov and N.Z. Lyakhov, Preparation and Sintering of Nanosized Alpha-Al_2O_3 Powder, *Nanostruct. Mater.*, 1999, **11**, p 559-572
4. H. Luo, D. Goberman, L. Shaw, and M. Gell, Indentation Fracture Behavior of Plasma-Sprayed Nanostructured Al_2O_3-13 wt.% TiO_2 Coatings, *Mater. Sci. Eng. A*, 2003, **346**, p 237-245
5. L.L. Shaw, D. Goberman, R. Ren, M. Gell, S. Jiang, Y. Wang, D.T. Xiao, and P.R. Strutt, The Dependency of Microstructure and Properties of Nanostructured Coatings on Plasma Spray Conditions, *Surf. Coat. Technol.*, 2000, **180**, p 1-8
6. Y. Wang, S. Jiang, M. Wang, S. Wang, T.D. Xiao, and P.R. Strutt, Abrasive Wear Characteristics of Plasma Sprayed Nanostructured Alumina/Titania Coatings, *Wear*, 2000, **237**, p 176-185
7. H.Y. Ding, Z.D. Dai, S.C. Skuiry, and D. Hui, Corrosion Wear Behaviors of Micro-Arc Oxidation Coating of Al_2O_3 on 2024Al in Different Aqueous Environments at Fretting Contact, *Tribol. Int.*, 2010, **43**, p 868-875
8. A.K. Keshri, J. Huang, W. Choi, and A. Agarwal, Intermediate Temperature Tribological Behavior of Carbon Nanotube Reinforced Plasma Sprayed Aluminum Oxide Coating, *Surf. Coat. Technol.*, 2010, **204**, p 1847-1855
9. X. Lin, Y. Zenga, C. Ding, and P. Zhang, Effects of Temperature on Tribological Properties of Nanostructured and Conventional Al_2O_3-3 wt.% TiO_2 Coatings, *Wear*, 2004, **256**, p 1018-1025
10. D. Yan, J. He, X. Li, Y. Liu, J. Zhang, and H. Ding, An Investigation of the Corrosion Behavior of Al_2O_3-Based Ceramic Composite Coatings in Dilute HCl Solution, *Surf. Coat. Technol.*, 2001, **141**, p 1-6
11. I. Ahmad, A. Kennedy, and Y.Q. Zhu, Wear Resistant Properties of Multi Walled Carbon Nanotubes Reinforced Al_2O_3 Nanocomposites, *Wear*, 2010, **269**, p 71-78
12. J.W. An, D.H. You, and D.S. Lim, Tribological Properties of Hot-Pressed Alumina-CNT Composites, *Wear*, 2003, **255**, p 677-681
13. K. Balani, S.P. Harimkar, A.K. Keshri, Y. Chen, N.B. Dahotre, and A. Agarwal, Multiscale Wear of Plasma-Sprayed Carbon-Nanotube-Reinforced Aluminum Oxide Nanocomposite Coating, *Acta Mater.*, 2008, **56**, p 5984-5994
14. D.S. Lim, J.W. An, and H.J. Lee, Effect of Carbon Nanotube Addition on the Tribological Behavior of Carbon/Carbon Composites, *Wear*, 2002, **252**, p 512-517
15. D.S. Lim, D.H. You, H.J. Choi, S.H. Lim, and H. Jang, Effect of CNT Distribution on Tribological Behavior of Alumina-CNT Composites, *Wear*, 2005, **259**, p 539-544
16. A.K. Keshri, R. Patel, and A. Agarwal, Comprehensive Process Maps to Synthesize High Density Plasma Sprayed Aluminum Oxide Composite Coatings with Varying Carbon Nanotube Content, *Surf. Coat. Technol.*, 2010, **205**, p 690-702
17. G.R. Anstis, P. Chantikul, B.R. Lawn, and D.B. Marshall, A Critical Evaluation of Indentation Techniques for Measuring Fracture Toughness: Direct Crack Measurements, *J. Am. Ceram. Soc.*, 1981, **64**, p 533-538
18. J. Wang, F. Yana, and Q. Xue, Tribological Behavior of PTFE Sliding Against Steel in Sea Water, *Wear*, 2009, **267**, p 1634-1641
19. X. Wang, N.P. Padture, and H. Tanaka, Contact-Damage-Resistant Ceramic/Single-Wall Carbon Nanotubes and Ceramic/Graphite Composites, *Nat. Mater.*, 2004, **3**, p 539-544
20. G.D. Zhan, J.D. Kuntz, J. Wan, and A.K. Mukherjee, Single Walled Carbon Nanotube as Attractive Toughening Agents in Alumina Based Nanocomposites, *Nat. Mater.*, 2003, **2**, p 38-42
21. G.D. Quinn and R.C. Bradt, On the Vickers Indentation Fracture Toughness Test, *J. Am. Ceram. Soc.*, 2007, **90**, p 673-680
22. S.S. Kim, Y.H. Chae, and D.J. Kim, Tribological Characteristics of Silicon Nitride at Elevated Temperatures, *Tribol. Lett.*, 2000, **9**, p 227-232
23. J. Li and D. Xiong, Tribological Behavior of Graphite-Containing Nickel-Based Composite as Function of Temperature, Load and Counterface, *Wear*, 2009, **266**, p 360-367
24. S. Wilson and A.T. Alpas, Dry Sliding Wear of a PVD TiN Coating Against Si_3N_4 at Elevated Temperatures, *Surf. Coat. Technol.*, 1996, **86-87**, p 75-81
25. FACTSAGE, *Thermodynamic Equilibrium Software, Version 5.0*, Center for Research in Computational Thermochemistry of

the Ecole Polythechnique at the Université de Montréal and GTT-Technologies, GmbH, Aachen, Germany, 2001
26. Y.S. Feng, S.M. Zhou, Y. Li, and L.D. Zhang, Preparation of the SnO_2/SiO_2 Xerogel with a Large Specific Surface Area, *Mater. Lett.*, 2003, **57**, p 2409-2412
27. N. Koshizaki, H. Umehara, and T. Oyama, XPS Characterization and Optical Properties of Si/SiO_2, Si/Al_2O_3 and Si/MgO Co-Sputtered Films, *Thin Solid Films*, 1998, **325**, p 130-136
28. S. Osswald, M. Havel, and Y. Gogotsi, Monitoring Oxidation of Multiwalled Carbon Nanotubes by Raman Spectroscopy, *J. Raman Spectrosc.*, 2007, **38**, p 728-736
29. C. Li, D. Wang, T. Liang, X. Wang, J. Wu, X. Hu, and J. Liang, Oxidation of Multiwalled Carbon Nanotubes by Air: Benefits for Electric Double Layer Capacitors, *Powder Technol.*, 2004, **142**, p 175-179
30. A.G. Evans and B. Marshall, Wear Mechanism in Ceramics, *Fundamentals of Friction and Wear of Materials*, D.A. Rigney, Ed., ASM International, Metals Park, OH, 1981, p 439-452